

Received June 2, 2016, accepted June 12, 2016, date of publication June 16, 2016, date of current version July 22, 2016.

Digital Object Identifier 10.1109/ACCESS.2016.2581844

Mine Safety System Using Wireless Sensor Network

VALDO HENRIQUES AND REZA MALEKIAN, (Member, IEEE)

Authors contributed equally to this work

Department of Electrical, Electronic and Computer Engineering, University of Pretoria, Pretoria 0002, South Africa

Corresponding author: R. Malekian (reza.malekian@ieee.org)

This work was supported in part by the National Research Foundation under Grant IFR160118156967 and in part by the Research Development Program, University of Pretoria under Grant AOX220.

ABSTRACT This paper describes the work carried out on the design and construction of a mine safety system prototype using a wireless sensor network with the objective of building a safety system to monitor the ambient characteristics of the mining environment. A review of the current literature relating to the health and safety of mine workers and mine safety systems is done. The subsystems of the prototype system are then simulated. The hardware consisted of electronic circuitry where a microcontroller is the principal processing unit. A graphical user interface is also implemented. A number of qualification tests are carried out. The temperature, humidity, airflow, and noise sensor measurements have an accuracy of 89.01%, 98.55%, 90.5%, and 89.53%, and a resolution of 0.105 °C, 0.12% RH, 0.05 m/s, and 0.23 dB SPL, respectively. In addition, gas and dust sensors met the specification; however, the accuracy could be improved. Two controlled outputs were implemented in the form of ventilation switching and a noise protection scheme.

INDEX TERMS Mining industry, sensor systems, temperature measurement, humidity measurement, airflow measurement, noise sensor measurement, wireless sensor networks, Zigbee.

I. INTRODUCTION

Mining as defined by the Oxford Dictionary is the process or industry of obtaining coal or other minerals from a mine. The activities carried out in order to obtain these minerals have a dangerous element to them. The average mine worker is exposed to the harsh underground environment which can sometimes incur an injury or cause loss of life. A portion of these injuries/fatalities can be attributed to human error.

However, there are circumstances that are dictated by the ambient conditions underground which can be blamed for these accidents. These conditions are difficult to monitor without placing someone's life at risk. The older methods of mine condition monitoring involved using a person to go down and report back. This method is however dangerous as the person who is monitoring a specific hazard could be harmed by that very same hazard [1]. This type of first hand monitoring is invasive.

There is an existence of specific systems or schemes which are put into place for these hazardous environments in order to protect the worker from harm. The higher level term for these systems/schemes is the Occupational Health and Safety. The International Organization of Standardization or ISO have a standard namely the ISO 45001. This standard aims to reduce the liability of occupational injuries and diseases not only

to benefit the workers but also the economy upon which this work builds [2]. These accidents can lead to losses due to early retirements and increased insurance premiums for the mine. The cooperation of this standard is crucial and is observed by the certification to a majority of the major mining companies in South Africa. This standard can be reinforced through the implementation of modern technology alongside policies to obtain the best possible result.

The technology which is central to the implementation of a non-invasive mine safety system is wireless sensor networks. These networks work by reading some data and transmitting these to a central computer or processing terminal for post processing. There are a number of sensor nodes [3], [4] which reside in different locations and communicate with each other [5], [6]. The method of communication is largely dependent upon the network topology or architecture that is implemented. The two main topologies which will be considered in the scope of this project is the mesh and star network topologies. A mesh topology sees each node connected to a minimum of two nodes. The star network sees each node connected to a hub or central node; therefore each node can only communicate with this hub directly. The use of wireless sensors networks provide a variety of advantages including but not limited to a reduction of wiring [7],

ease of implementation and it provides a non-invasive method of monitoring the state of the mine's conditions i.e. monitoring without having to expose a person to the potentially hazardous environment. In addition to these, control can be imposed on the environment from a remote location allowing a person to interact with the surrounding environment without having to be in that environment.

In order to successfully communicate raw data, this data must first be measured through the use of sensors. These sensors measure analog voltage values based upon specific ambient characteristics. The applications of sensors are vast in that there are a large number of characteristics which can be measured. The utility of sensors is apparent in applications where the characteristic measurement is required in real-time [8]. The characteristics measured in this project include: (i) temperature, (ii) air-flow, (iii) humidity, (iv) noise, (v) dust and (vi) gas concentration. Each of these characteristics can be solely or collectively responsible for incurring a risk to a mine worker.

The growth of mineral resources as an emerging and existing economic sector, the increase in mining activity has become essential to this sector and to the economies these markets are built on. The practice of mining can be dangerous [9] and unsafe. The previous statement is only true for mines that do not monitor conditions inside the mine. There exists a relationship between three entities namely a hazard, latent danger and an accident which find their existence due to this dangerous and potentially unsafe practice. This relationship is illustrated in figure 1 below.

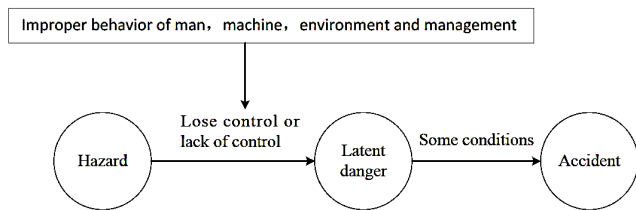


FIGURE 1. Relationship between a hazard, latent danger and an accident [10].

The system was completely designed from first principles, this includes the sensor hardware, device hardware, PCB layout, software algorithms, as well as a graphical user interface. The proposed system designed examines and implements certain functionality that solves the above-mentioned shortcomings or limitations in real-time mining environment monitoring [11]. The system allows for monitoring of multiple different zones inside the mine, the protection of mine workers from excessive noise levels and the storage of measurement data for purposes of reference.

Background on current methods of obtaining and processing the mentioned ambient characteristics has been discussed. Next the system overview from a high level perspective will be discussed. The results presented from this system show its validity. These results are then used as the basis for the discussion and conclusion.

This paper is organised as follows. Section II discusses the system components and the containing interfaces. Section III provides a summarised description of the prototype system's implementation. The findings and results are summarised in section IV. Section V provides suggestions for future work and possible system improvements. Finally, the paper is concluded in section VI.

II. SYSTEM OVERVIEW

Figure 2 shows A high level overview of the system. This figure shows that the system consists of two subsystems known as the two nodes of the system.

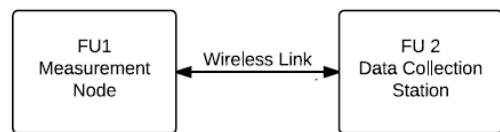


FIGURE 2. Wireless based mine safety system functional level diagram.

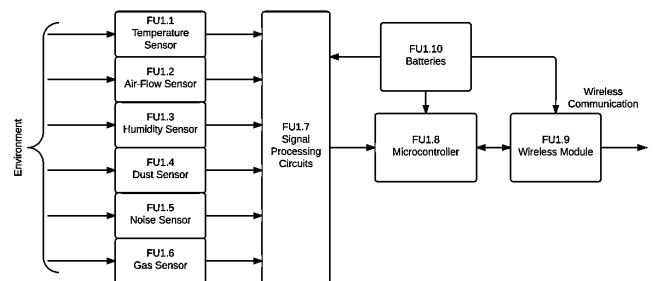


FIGURE 3. Sensor node functional level diagram.

From Figure 3 the most important component of the system is the measurement node (FU1). This component should be responsible for all measurements made. The measurement node should contain many different sensors that will return values such as gas concentration, temperature, humidity, air flow and noise levels. These values should then be transferred via a wireless link to data collection station (FU2); this station will have the necessary hardware (a wireless module and a microcontroller, interfaced to a laptop computer) and software to perform the required processing, displaying and storage of values. In addition to this the data collection station is also responsible for producing a safety scheme for workers using the values collected. The measurement node and the data collection node should communicate only via the ZigBee wireless protocol.

The array of different sensors is the epicenter of this project without which the creation of the desired system would be illogical. The ambient conditions provided are fed into the sensors. The temperature (FU1.1), air-flow (FU1.2) and humidity (FU1.3) sensors are created from first principles. The most important of these is the air flow sensor which will detect the amount of air movement inside the mine. The dust (FU1.4), noise (FU1.5) and gas (FU1.6) sensors are off-the-shelf components with signaling design. Each of

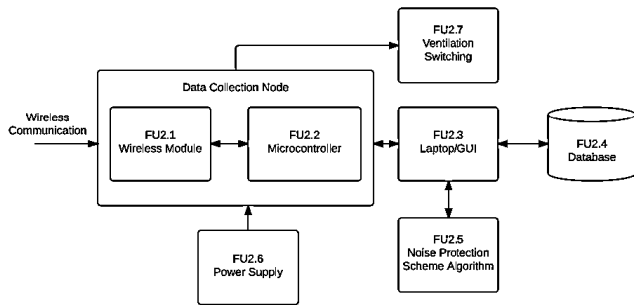


FIGURE 4. Collection node functional level diagram.

the sensors will interface with their own respective signal processing circuits (FU1.7). These circuits will provide the necessary conditions to obtain the required output from the sensors. The signals/values that are obtained from these sensors should be sampled by the microcontroller (FU1.8). This microcontroller is the central processing unit or controller of the measurement node. The values input to and output by the microcontroller will determine operation of other functional units. A timer will be placed onto the microcontroller to represent the delay between each sample taken from the respective sensors. A wireless module (FU1.9) will be interfaced with the microcontroller to transmit the sensor data across to the data collection station. This module will use the ZigBee 802.15.4 wireless protocol. The measurement node should be powered by batteries (FU1.10). This is to enable the measurement node to be mobile which is necessary if the entire mine is to be measured.

The sensor data measured by the measurement node in Figure 4 is communicated to the data collection node which consists of the second wireless module (FU2.1) and the second microcontroller (FU2.2). This is the necessary hardware required to communicate the sensor data to the laptop computer/GUI (FU2.3). The visual illustration of testing data is vital to the project’s outcomes and overall impression. The GUI (FU2.3) will display the values which originate from the measurement node (FU1). These values are originally input to the laptop via the USB interface from the microcontroller’s (FU2.2) output commands. The data collection node should be powered by a power supply (FU2.6). The power supply unit should take the domestic voltage supply (220 – 240 V_{ac}) and convert it to two smaller DC voltages which will power this node. Depending on the conditions measured by the air-flow and gas sensors, a ventilation switching module (FU2.7) will be controlled. Another functional unit that interfaces with the GUI will be called the noise protection scheme algorithm (FU 2.5). This unit is the module which will provide the noise protection scheme depending on past and present values obtained from the measurement node. The values obtained from testing should also be stored in a database format. Records of the values measured should be stored in a Database (FU2.4). This database will allow for the comparison between past and present testing results which should be used to evaluate the state of the mines safety conditions.

III. SYSTEM DESIGN

A. TEMPERATURE SENSOR

This is the sensor which is used to measure the ambient air temperature inside the mine. This sensor was built from first principles using a load balanced thermistor circuit. This circuit acts as a voltage divider between the thermistor and the applied resistor (load). A thermistor is a temperature dependent variable resistor. Although all resistors are sensitive to temperature changes, thermistors are especially sensitive to temperature due to the material it is constructed from. This material has a specific resistivity. This resistivity is a constant for that material. The temperature sensor circuit is shown in figure 5.

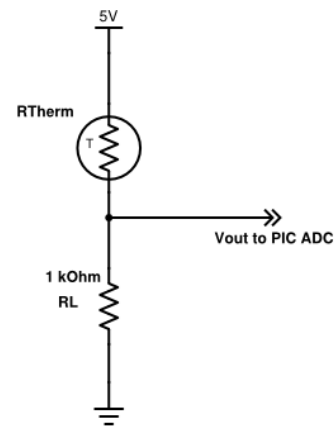


FIGURE 5. Temperature sensor circuit schematic.

The thermistor used has a resistance of 2000 ohms at 25 °C. Before the load resistor value choice is justified, the process of calibration and measurement from this sensor will be elaborated. The 3-Point calibration method was used. This involves measuring the resistance of the thermistor at 3 different temperatures. Solving for the thermistors characteristic constants, the following values were found

$$\begin{aligned}
 k_a &= 1.692 \times 10^{-3} \\
 k_b &= 1.896 \times 10^{-4} \\
 k_c &= 4.602 \times 10^{-7}.
 \end{aligned}$$

These constants are used for the conversion of the resistance of the thermistor to the ambient temperature output. This is achieved using the Steinhart equation shown in equation 1

$$T = \frac{1}{[k_a + (k_b \times \ln R_t) + k_c \times (\ln R_t)^3]} - 273.15 \quad (1)$$

where T = Temperature (°C) and R_t = Thermistor Resistance (Ω).

The equation which governs the relationship between the voltages measured by the microcontroller’s analogue to digital converter and the thermistor’s resistance is given by equation 2.

$$V_{out} = V_{supply} \times \left(\frac{R_L}{R_L + R_{Therm}} \right) \quad (2)$$

This equation is simply the voltage divider equation which will now be used to determine the thermistor's varying resistance R_{Therm} . In order to determine this value the following mathematical manipulation was required.

$$\frac{V_{out}}{V_{supply}} = \left(\frac{R_L}{R_L + R_{Therm}} \right)$$

$$\frac{V_{out}}{V_{supply}} \times (R_L + R_{Therm}) = R_L$$

$$R_L + R_{Therm} = R_L \times \frac{V_{out}}{V_{supply}}$$

$$R_{Therm} = R_L \times \frac{V_{out}}{V_{supply}} - R_L$$

$$R_{Therm} = R_L \times \left(\frac{V_{out}}{V_{supply}} - 1 \right) \quad (3)$$

This result was then used in the Steinhart equation to determine the temperature from the resistance of the thermistor. The result of this has been simulated in MATLAB and is shown below in figure 6.

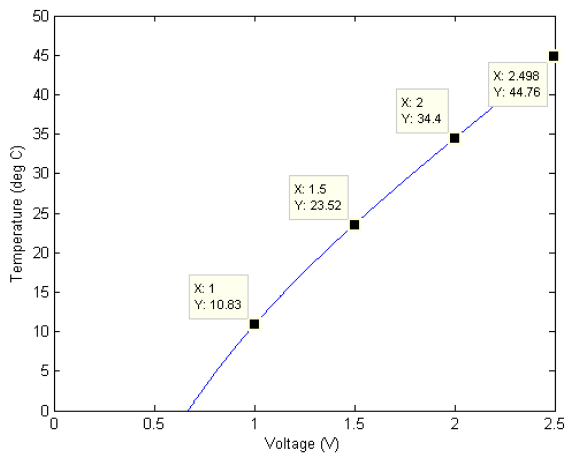


FIGURE 6. Temperature sensor voltage relationship.

In order to find the correct load to provide the best range of measurement, a range of different values were simulated for the load. It was found that a 1000 ohm resistor was best.

B. HUMIDITY SENSOR

This is the sensor which is used to measure the ambient humidity inside the mine. This sensor has a typical current draw of 200 μA [12] which makes it ideal for a battery operated system. This sensor produces a varying voltage depending upon the ambient water vapour exposed to the sensor. The output voltage produced from the sensor has a range of 0.8V – 3.8V. As the microcontroller used to measure these values has an operating voltage of 5V, this range can be extended. An additional piece of hardware is designed to achieve this. This piece of hardware is a non-inverting operational amplifier. This operational amplifier is used to add the required gain to increase the output range. By adding this gain, the resolution of the humidity measurement is

made larger. Figure 7 shows the circuit schematic for the humidity sensor.

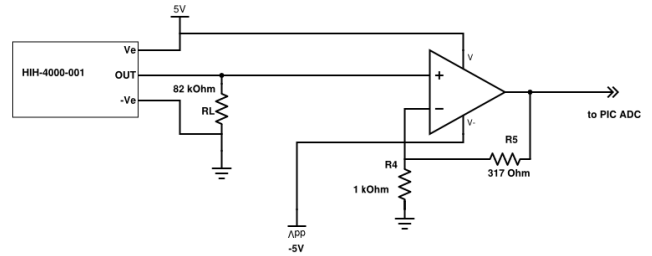


FIGURE 7. Humidity sensor circuit schematic.

In order to extend the output voltage range to the 5V level. The gain was calculated using equation 4

$$Gain = \frac{5V}{Current\ Maximum} = \frac{5}{3.8} = 1.317 \quad (4)$$

This gain was achieved by using the non-inverting operational amplifier which has a characteristic equation as shown in equation 5

$$V_{OUT} = V_{IN} \left(1 + \frac{R5}{R4} \right) \quad (5)$$

Therefore R5 is chosen as 317 Ω and R4 as 1k Ω to achieve the required output range. RL is chosen to be 80k Ω as the sensor needs a minimum of 80k Ω from the output to the negative pin to produce the correct output [12].

The humidity sensor produces an output voltage which relates to the RH (relative humidity) according to equation 6.

$$V_{OUT} = V_{SUPPLY} (0.0062 (Sensor\ RH) + 0.16) \quad (6)$$

This equation is manipulated to find the equation which would use voltage output as the input variable and the sensor RH as the output. This result is shown in equation 7.

$$Sensor\ RH = \frac{\frac{V_{OUT}}{V_{SUPPLY}} - 0.16}{0.0062} \quad (7)$$

As a result of adding this gain the output voltage range differs and is shown on figure 8.

In addition to the change in the range of measurement, the resolution has been improved as well. Using the observed data cursors in figure 8, a change of 0.5V is shown on both lines. If the sensor is to be used without gain, this difference corresponds to 16.28% RH. The sensor with the additional gain shows a corresponding difference of 12.37% RH. To directly compare, these humidity values will be divided by the voltage to give the humidity per voltage value.

$$Without\ Gain = \frac{16.28}{0.5} = 32.56\ RH/V$$

$$With\ Gain = \frac{12.37}{0.5} = 24.74\ RH/V \quad (8)$$

The result of directly comparing these leads to the conclusion that the sensor with additional gain has a higher resolution. This will benefit the system by allowing for measurements to be made with a higher degree of accuracy.

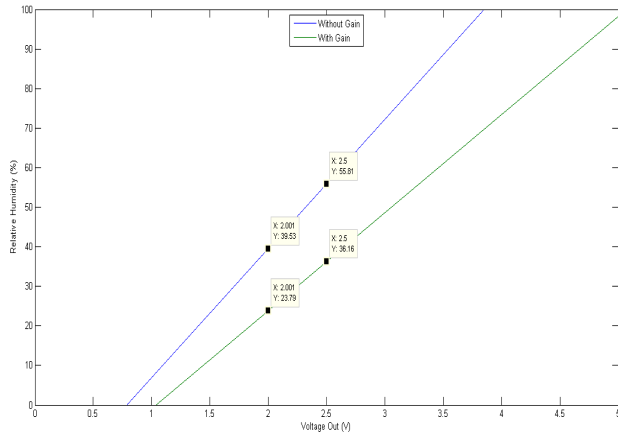


FIGURE 8. Humidity sensor voltage relationship.

C. AIRFLOW SENSOR

This is the sensor which is used to measure the ambient airflow inside the mine. This sensor was built from first principles utilizing a slotted optical switch in conjunction with a 3 cup anemometer. This functional unit will therefore be discussed in two parts, one part for the design and implementation of the electronic component and another for the design and implementation of the mechanical cup anemometer.

A slotted optical switch is a component which consists of an LED and a phototransistor. The LED emits a near infrared light directly through a small aperture towards the phototransistor. The slotted optical switch used in this design is the OPB804. Upon detecting this light, the transistor will activate and switch on thus the voltage level changes from low to high. The schematic in figure 9 on the following page illustrates the circuit used for the airflow sensor.

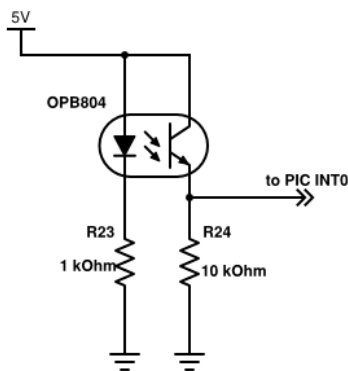


FIGURE 9. Airflow sensor circuit schematic.

The resistance value of R₂₃ is chosen to be 1kΩ; it is used as a current limiting resistor to protect the optical switch’s LED. The current flowing through the LED is 5/1000 = 5 mA which is below the maximum rating of the optocoupler which is 50 mA. The resistor R₂₄ is chosen to be 10kΩ as the output of the optical switch will be input as a high or low level voltage value to the microcontroller. This pull down resistor allows for the value to settle at the appropriate level. The optical switch works in conjunction with a small

piece of metal mounted onto the bearing of the anemometer. As the anemometer rotates, this metal interrupter crosses the slot of the slotted optical switch. Each time this piece crosses the slot one revolution has been observed.

The microcontroller has a timer which is used to calculate the corresponding RPM by using equation 9.

$$RPM = \frac{60}{\text{Number of Ticks} \times 0.001} \tag{9}$$

Here the timer produces a number of ticks between each interrupt signal. The timer has been setup such that each clock cycle is 0.001 seconds. Each minute contains 60 seconds and the duration between each interrupt forms the divider to produce the number of revolutions per minute. Once the number of revolutions per minute has been found, the theoretical linear speed can be found using equation 10.

$$\text{Linear Speed} = RPM \times r \times \frac{2\pi}{60} \tag{10}$$

where r = Anemometer Radius (m).

The anemometer’s rotational diameter was designed to be 0.25m.

The resulting relationship was plotted and compared against the theoretical relationship given in equation 8 and is shown in figure 10.

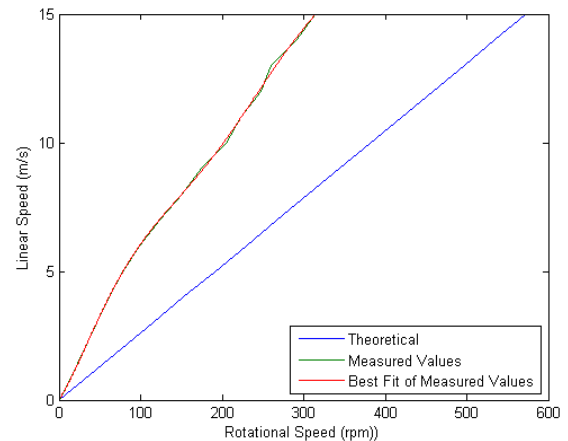


FIGURE 10. Airflow sensor response.

The final response obtained for the airflow sensor is given in equation 11.

$$\begin{aligned} \text{Linear Speed} = & 0.00000000000142 \times RPM^6 \\ & - 0.000000000157159 \times RPM^5 \\ & + 0.000000064166852 \times RPM^4 \\ & - 0.000011559090677 \times RPM^3 \\ & + 0.000781822703426 \times RPM^2 \\ & - 0.048124238198520 \times RPM \\ & + 0.010938918326562. \end{aligned} \tag{11}$$

A cup type anemometer is chosen because the cup type anemometer is rapid in responding to the fluctuations of



FIGURE 11. Noise sensor functional level diagram.

wind speed across the structure. This type of anemometer is inexpensive and uses a proportional relationship to produce its output. The three most important parameters when considering the design of an n-cup anemometer is the radius of rotation, the number of cups used and the radius of the cups used in the design.

Upon reading up on anemometers and the number of cups, the final number of cups are chosen to be three cups. This is due to the fact that the 3 cup anemometer has a faster response to fluctuations than a 4 cup anemometer and also provides a more uniform response [13]. This in turn means that each cup is mounted at intervals of 120° of a uniform circle.

D. NOISE SENSOR

This is the sensor which is used to measure the ambient sound level inside the mine. This sensor is named a noise sensor only due to the nature of the sound that is being measured. This sensor measures the sound level inside the mine that would be considered noise because of its effect on the employees. Figure 11 shows the high level functional diagram of the noise sensor’s design.

The input transducer for this sensor is an electret microphone. The microphone’s output provides the input to the filter and amplification circuit. Finally to obtain a constant voltage value which can be accurately measured by the microcontroller a peak detector was used.

The filtering stage included a band pass filter for the frequency range of 20Hz to 20kHz. This is done so as to filter for signals in the audible frequency range.

The noise sensor calibrated and the resulting relationship is plotted and is shown in figure 12.

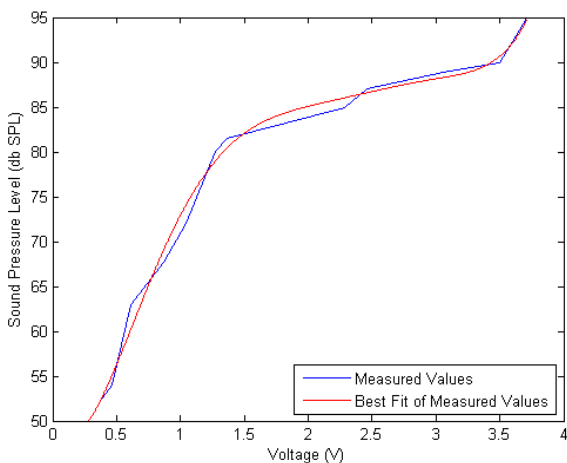


FIGURE 12. Noise sensor response.

The final mathematical relationship between the voltage and the sound pressure level is extracted from this plot and is shown in equation 12.

$$\begin{aligned}
 \text{Sound Pressure} = & 0.9165 \times V^6 - 11.4017 \times V^5 \\
 & + 55.5430 \times V^4 - 130.52 \times V^3 \\
 & + 140.288 \times V^2 - 32.5324 \times V \\
 & + 50.6647. \tag{12}
 \end{aligned}$$

E. GAS SENSOR

This is the sensor which is used to measure the ambient gas concentration inside the mine. The component used for this design is the Figaro TGS2611-C00. This sensor is used to detect the concentration of methane in the air of the mine. Methane is an asphyxiate gas and it is flammable. The detection of this gas is vital to the protection of mine worker’s health. This sensor is of the semiconductor type with an integrated heating element and consumes a low amount of current at 56mA for the heater [14]. The circuit schematic for the gas sensor is shown in figure 13.

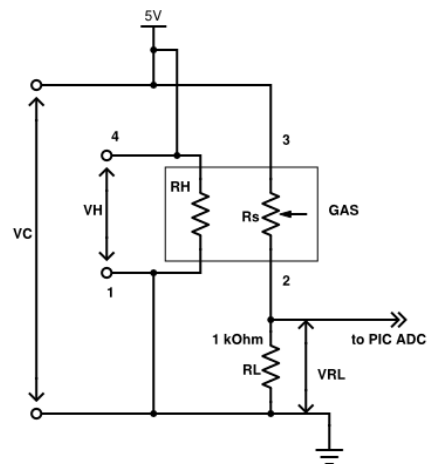


FIGURE 13. Gas sensor circuit schematic.

The load resistor R_L is chosen to meet the minimum load resistor requirement for the sensor [15] which is 0.45kΩ. The gas sensor acts as a voltage divider whereby the circuit voltage V_C is divided across R_S and R_L . As the gas concentration changes the value of R_S changes. To obtain the resistance of the sensor R_S , it is necessary to first measure the voltage across the load resistor. Once this voltage has been measured the value of R_S can be found using equation 13

$$R_S = \frac{V_C - V_{RL}}{V_{RL}} \times R_L \tag{13}$$

The value of R_S is the first step to converting the voltage measured across the load resistor to a methane concentration. The value of R_0 is 2.3kΩ; this is the resistance of the sensor in 5000ppm (parts per million) of methane. As shown by figure 14, the sensors relationship is governed by the value of R_S/R_0 .

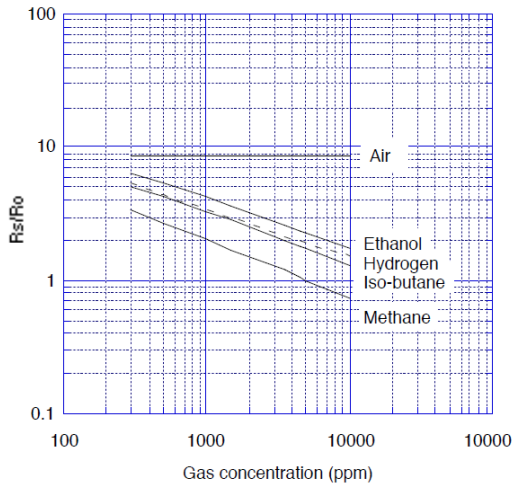


FIGURE 14. Gas sensor characteristic response.

Using knowledge of logarithmic graphs together with the graph intercept method, a relation is derived for the line in figure 14. This relation is given by equation 14:

$$\frac{R_S}{R_o} = 41.792 \times ppm^{-0.43987} \tag{14}$$

This equation is then manipulated in order to make the concentration (ppm) the subject of the equation. This resulted in equation 15.

$$ppm = \left(\frac{R_S}{R_o \times 41.792} \right)^{-2.273} \tag{15}$$

This is the final equation used to convert the measured voltage into a gas concentration in parts per million.

F. DUST SENSOR

This is the sensor which is used to measure the dust concentration inside the mine. This sensor comprises the use of an off the shelf component and some additional hardware to facilitate measurement. The sensor used to detect dust in this design is the Sharp GP2Y1010AU0F. This sensor is an optical type dust sensor. This means that the sensor uses detected light intensities to measure the dust concentration in the air. It has a current consumption of 10mA [16]. To obtain the correct output from this sensor, the sensor needs to be connected as shown in figure 15.

To obtain an output waveform from the sensor, the sensor requires a square wave input. This is achieved using the PWM output from the microcontroller. This PWM output is used to drive the LED inside the sensor. R22 and C11 are the recommended values that need to be used [16]. Figure 16 shows the required signal needed to drive the sensor.

The sensor has a voltage sensitivity of 0.5V per 0.1mg/m³ and 0.9V output when there is no dust [16]. This offset will be subtracted from the voltage measured on the microcontroller.

G. NODES AND GRAPHICAL USER INTERFACE

The sensor node is battery powered while the collection node used a power supply. This fits with the theme of their

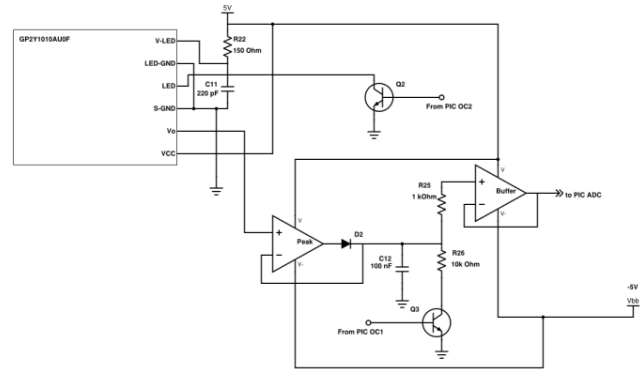


FIGURE 15. Dust sensor circuit schematic.

Pulse-driven wave form

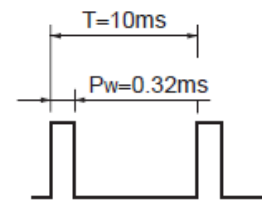


FIGURE 16. Dust sensor led drive signal.



FIGURE 17. Collection node.

individual application. Due to the fact that the sensor node needed to be mobile it is battery powered. The collection node being stationary could be powered with a suitable power supply. Each node made use of a dsPIC30F4011 which contained the required functions both in hardware and software to fulfil the requirements of the system. The measurement parameters are exchanged between the nodes via a ZigBee interface. The nodes are shown in figures 17 and 18.

The graphical user interface was used as the visual output of the measurement parameters. In addition, the noise protection scheme is part of the graphical user interface. The noise protection scheme provides a visual output of the noise levels in particular zones of the mine. This is used to help the mine engineer to make an executive decision on whether or not it is safe to send a worker to that particular zone. A screenshot of the noise protection scheme is shown in figure 19.

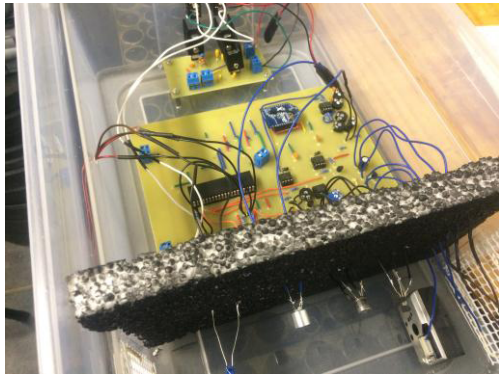


FIGURE 18. Sensor node.

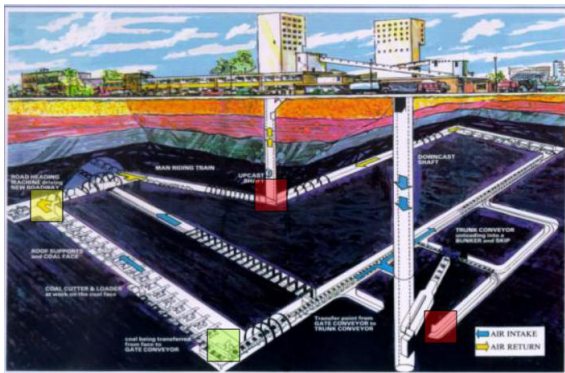


FIGURE 19. Noise protection scheme.



FIGURE 20. Temperature sensor test setup.

IV. RESULTS AND OBSERVATIONS

The system is put through a series of tests. Each test had a focus on a specific subsystem. These results are summarized in table 1.

The following figures show the setup used to test each of the sensors. These tests involved the use of a calibrated reference meter that is used to compare against the measured value.

The range of measurement of the temperature sensor (Fig.20) exceeds the stated specification. The obtained range

TABLE 1. System results.

Intended Outcome	Actual Outcome
Temperature Sensor should have a <ul style="list-style-type: none"> - Range = 20 - 35°C - Resolution = 0.5°C 	Temperature Sensor has a <ul style="list-style-type: none"> - Range = 2 - 45°C - Resolution = 0.105°C Accuracy = 89.01%
Humidity Sensor should have a <ul style="list-style-type: none"> - Range = 0 – 90% - Resolution = 5% 	Humidity Sensor has a <ul style="list-style-type: none"> - Range = 0 – 100% - Resolution = 0.12% Accuracy = 98.55%
Airflow Sensor should have a <ul style="list-style-type: none"> - Range = 0 m/s – 15m/s - Resolution = 0.5m/s 	Airflow Sensor has a <ul style="list-style-type: none"> - Range = 0 m/s – 15m/s - Resolution = 0.05m/s Accuracy = 90.5%
Noise Sensor should have a <ul style="list-style-type: none"> - Range = 0 – 95dB SPL - Resolution = 5dB SPL 	Noise Sensor has a <ul style="list-style-type: none"> - Range = 50 – 95dB SPL - Resolution = 0.23dB SPL Accuracy = 89.53%
Gas (CH ₄) Sensor should have a <ul style="list-style-type: none"> - Range = 0 – 70ppm - Resolution = 1ppm 	Gas (CH ₄) Sensor has a <ul style="list-style-type: none"> - Range = 0 – 2554.75ppm - Resolution = 0.9ppm Accuracy = undetermined
Dust Sensor should have a <ul style="list-style-type: none"> - Range = 0 – 10mg/m³ - Resolution = 0.5 mg/m³ 	Dust Sensor has a <ul style="list-style-type: none"> - Range = 0 – 0.554mg/m³ - Resolution = 0.003 mg/m³ Accuracy = undetermined
The wireless communication should have a maximum range of 50 m.	The wireless communication has a maximum range of 51.1m indoor and 150m outdoor.
All data captured and transmitted to the GUI should be recorded within a database allowing for all historical information to be viewable at a later stage.	System is able to recall historical data with 100% accuracy.

is 2 – 45°C which exceeds the specification in the lower range by 18°C and in the higher range by 10°C. The expansion in range allows for a wider array of temperature to be measured. While the lower expansion is appreciated, it is the expansion of the range at the higher limit which is more useful to the operation of this system. It is not likely to find a temperature lower than 20°C in the mining environment; however there exists a possibility that the temperature could exceed 35°C. Therefore this extended range is applicable and enhances the temperature sensing capabilities of the prototype system. The obtained resolution is 0.105°C compared to the specified 0.5°C. This result exceeds the specification and is therefore good as this increases the number of different temperature values that can be measured over the range.

In addition to the range and resolution, accuracy is another metric which has a high level of importance when considering measurement. Although accuracy is not part of the specification for any of the sensors, it will be discussed here to provide the highest level of transparency. The worst case accuracy of the temperature sensor is 89.01% although this is an acceptable result. The accuracy can however be improved. During the 3-point calibration step, a set of measurements pertaining to the resistance of the thermistor and the temperature were made. The reference temperature measurement is made using a digital thermometer which is part of an alarm clock. While this thermometer provided the necessary measurements, its level of accuracy can now be called into question. In order to improve the accuracy of this sensor, a precision digital thermometer should be used for the 3-point calibration process. This loss in accuracy is a compromise for the fast reacting nature of this temperature sensor design.



FIGURE 21. Humidity sensor test setup.

The range of measurement of the humidity sensor (Fig.21) exceeds the stated specification. The obtained range is 0 – 100% which exceeds the specification in the higher range by 10%. The indicated result is very good. This result is important as the level of relative humidity between 90% and 100% can cause risk to the productivity of the mine with the existence of water vapor in large quantities. At this level of humidity the human body no longer sweats. This lack of sweat means that the body can no longer regulate its temperature, at which point there are serious health implications to the mine worker. Therefore this extended range is applicable and enhances the humidity sensing capabilities of the prototype system. The obtained resolution is 0.12% compared to the specified 5%. This result exceeds the specification and is therefore good as this increases the number of different humidity values that can be measured over the range. In addition to the range and resolution, accuracy is another metric which has a high level of importance when considering measurement. The accuracy of the humidity sensor is 98.55%.



FIGURE 22. Airflow sensor test setup.

The range of measurement of the airflow sensor (Fig.22) meets the stated specification of 0-15m/s. This is also considered as a good result. This result however holds an accuracy of 90.5%. While there is a higher level of error (worst case accuracy of 85.4%), this error is most applicable to the upper range of measurement (>10m/s). This accuracy is not acceptable and needs improvement. A reduction in accuracy of the airflow sensor can be seen as the magnitude of the airflow increases. At 5m/s the accuracy is 97.6%. This then reduces to 90% at 10m/s and finally to the worst case of 85.4% at 15m/s. This reduction of accuracy is due to the design of the cup anemometer. The anemometer used lightweight materials for the rotor design. At high magnitude of airflow, these lightweight materials cause vibration of the rotor. This vibration blocks the proper rotational response from the bearing of the rotor. This then results in the rotational speed of the rotor to decrease. This in turn means that the rotor has the potential to rotate faster but cannot in this setup due to the vibrational forces at higher magnitudes of airflow. This is why the level of accuracy is higher at the lower magnitudes of airflow, as the airflow is not large enough to cause lossy rotation. The upper range of this specification namely the level of airflow at 15m/s is classified as a light gale force wind. It is unlikely that this level of airflow will be experienced in the mining environment. However, the level of repeatability of the system is high. This pertains to the fact that if a specific airflow is exposed to the airflow sensor, it is likely to measure approximately the same value with small variance. The obtained resolution was 0.05m/s compared to the specified 0.5m/s. This result exceeds the specification and is therefore good as this increases the number of different airflow values that can be measured over the range.

The range of measurement of the noise sensor (Fig.23) meet the stated specification of 0-95 dB SPL. The measured range is 50-95 dB SPL. The obtained resolution is 0.23 dB SPL compared to the specified 5 dB SPL. This result exceeds the specification and is therefore good as this increases the number of different noise values that can be measured over



FIGURE 23. Noise sensor test setup.

the range. The accuracy of the noise measurement is 89.53%. The functioning of the noise sensor is heavily reliant on the calibration of the sensor. By using the noise sensor with a constant sound pressure being applied, a higher level of accuracy can be obtained. The calibration is also important because of the frequency spectrum of the applied sound pressure. If a set of sound pressures with differing frequency spectrums are applied, a different noise level will be determined. The best way to improve this calibration would be to sample the real sound which will be detected inside the mine, whether that is a jackhammer being used or an explosive.



FIGURE 24. Gas sensor test setup.

The range of measurement of the gas sensor (Fig.24) exceeds the stated specification. The obtained range is 0 – 2554.75ppm which exceeds the specification in the higher range by 2484.75ppm. This is also considered as a good result. The expansion in range allows for a wider array of gas concentration levels to be measured. It is the expansion of the range at the higher limit which is useful to the operation of this system. The TLV (threshold limit value) of methane as

a simple asphyxiate is 1000ppm [17]. The obtained resolution is 0.9ppm compared to the specified 1ppm. This result meets the specification and is therefore good as this slightly increases the number of different gas concentration values that can be measured over the range.

The obtained range of measurement of the dust sensor is 0 – 0.554mg/m³. The formula to find the concentration of the dust is shown in equations 16 [18]:

$$TLV = \frac{10mg/m^3}{\%Quartz + 2} \quad (16)$$

This formula limits the TLV to 0.1mg/m³. In addition to this, the 8-hour time-weighted limit of respirable dust as crystalline silica is 0.025mg/m³ [18]. This shows that the stated specification is over-specified for this particular application. The risk to health and safety inside the mine will happen at levels lower than 10 mg/m³. The measurement above the obtained range can therefore be seen as an acceptable result. The obtained resolution is 0.003mg/m³ compared to the specified 0.5 mg/m³. This result exceeds the specification and is therefore considered as good due to this increases the number of different dust values that can be measured over the range.

The wireless communication is also tested using two environments, the outdoor and indoor settings was used for these tests. The maximum range measured for the system using the outdoor setting was 150m. Note that this is the maximum value measured but the true maximum of line-of-sight communication using the wireless communication [19] in this system can be much larger. The maximum range measured in the indoor environment is 51.1m. This result meets the specification and is a good result. The access to historical data is paramount to operation of this system. This access to historical data allows for future decisions to be made. One example of this is the noise protection scheme which uses the past data of noise levels in each specific zone to produce a risk level.

V. FUTURE WORK

A major risk that can cause a large amount of damage in the mine environment is fire. An additional subsystem that could be considered for addition to the mine safety system is fire suppression. This would include the use of a smoke sensor and a controllable fire retardant system.

While the wireless communication implemented in this design shows success with urban/indoor communication, in order to enhance the system even further, multiple identical sensor nodes could be introduced. This would turn the master/slave (2 node star) topology into a mesh network. By using the proprietary technology from the manufacturer of the XBee module known as DigiMesh a smart mesh network can be configured. This would allow for a sensor node to be out of range with the collection node, but as long as that sensor node can communicate to another sensor node, the data can be passed along from the end sensor node to the collection node through intermediary sensor nodes. This would increase the communication range inside the mine.

VI. CONCLUSION

Therefore a complete mine safety system was constructed such that the system is compact and modular, using a combination of mechanical hardware, electronic hardware and specific software. This system can measure ambient characteristics inside the mine environment and communicate them between two nodes using the ZigBee communication protocol. The temperature, humidity, airflow and noise sensor measurements have an accuracy of 89.01%, 98.55%, 90.5%, 89.53% and a resolution of 0.105°C, 0.12% RH, 0.05m/s and 0.23 dB SPL respectively.

ACKNOWLEDGEMENT

Authors would like to thank Council for Scientific and Industrial Research (CSIR), South Africa for some advice during the course of this project.

REFERENCES

- [1] R. S. Nutter, "Hazard evaluation methodology for computer-controlled mine monitoring/control systems," *IEEE Trans. Ind. Appl.*, vol. IA-19, no. 3, pp. 445–449, May 1983.
- [2] *Occupational Health and Safety ISO 45001*, Int. Org. Standardization, UK, 2016.
- [3] X. Chen and P. Yu, "Research on hierarchical mobile wireless sensor network architecture with mobile sensor nodes," in *Proc. Int. Conf. Biomed. Eng. Informat.*, Oct. 2010, pp. 2863–2867.
- [4] P. Deshpande and M. S. Madankar, "Techniques improving throughput of wireless sensor network: A survey," in *Proc. Int. Conf. Circuit, Power Comput. Technol.*, Mar. 2015, pp. 1–5.
- [5] S. Kasera, N. Narang, and S. Narang, "Network topology and extent," in *Communication Networks: Principles and Practice*. New York, NY, USA: McGraw-Hill, 2005.
- [6] Y.-S. Choi, Y.-J. Jeon, and S.-H. Park, "A study on sensor nodes attestation protocol in a wireless sensor network," in *Proc. Int. Conf. Adv. Commun. Technol.*, Feb. 2010, pp. 574–579.
- [7] Y. K. Tan and K. Tseng, "Low-voltage, DC grid-powered LED lighting system with smart ambient sensor control for energy conservation in green building," in *Smart Grid Infrastructure & Networking*. New York, NY, USA: McGraw-Hill, 2013.
- [8] L. Yan-Fang *et al.*, "Fiber laser methane sensor and its application in coal mine safety," *Procedia Eng.*, vol. 26, pp. 1200–1204, Sep. 2011.
- [9] J. Dickens and R. Teleka, "Mine safety sensors: Test results in a simulated test stope," in *Proc. 6th Robot. Mechatronics Conf.*, Oct. 2013, pp. 105–110.
- [10] W. Bing, X. Zhengdong, Z. Yao, and Y. Zhenjiang, "Study on coal mine safety management system based on 'hazard, latent danger and emergency responses,'" *Procedia Eng.*, vol. 84, pp. 172–177, Nov. 2014.
- [11] R. S. Nutter, Jr., and M. D. Aldridge, "Status of mine monitoring and communications," *IEEE Trans. Ind. Appl.*, vol. 24, no. 5, pp. 820–826, Sep. 1988.
- [12] *HIH-4000 Series Humidity Sensor Datasheet*, Honeywell, Morris Plains, NJ, USA, 2010.
- [13] S. Pindado, J. Pérez, and S. Avila-Sanchez, "On cup anemometer rotor aerodynamics," *Sensors*, vol. 12, no. 5, pp. 6198–6217, 2012.
- [14] *TGS 2611—Methane Sensor Datasheet*, Figaro USA Inc., Arlington Heights, IL, USA, 2005.
- [15] *FTechnical Information for Methane Gas Sensors*, Technical Information for TGS2611, Figarosensors, USA, 2005.
- [16] S. Corporation, *GP2Y1010AU0F—Optical Dust Sensor Datasheet*, SHARP corporation, 2006.
- [17] *Association Advancing Occupational and Environmental Health, Material Safety Data Sheet-Natural Gas*, FortisBC, Canada, 2012.
- [18] *Lowell Institute for Mineral Resources, Crystalline Silica*, Univ. Arizona, Tucson, AZ, USA, 2011.
- [19] N. Ye, Y. Zhu, R.-C. Wang, R. Malekian, and L. Qiao-Min, "An efficient authentication and access control scheme for perception layer of Internet of Things," *Appl. Math. Inf. Sci.*, vol. 8, no. 4, pp. 1617–1624, 2014.



VALDO HENRIQUES received the B.Eng. degree in computer engineering from the University of Pretoria, South Africa. His research interests include advanced sensor networks.



REZA MALEKIAN (M'12) is currently a Senior Lecturer with the Department of Electrical, Electronic, and Computer Engineering, University of Pretoria, Pretoria, South Africa, and an Extraordinary Assistant Professor with the Departamento de Ingeniería Informática, Universidad de Santiago de Chile, Chile. His current research interests include advanced sensor networks, Internet of Things, and mobile communications. He is also a Chartered Engineer and a Professional Member of

the British Computer Society. He is an Associate Editor of the IEEE Internet of Things Journal.

• • •